Baseline/Postnitrate Tetrofosmin SPECT for Myocardial Viability Assessment in Patients with Postischemic Severe Left Ventricular Dysfunction: New Evidence from MRI

Assuero Giorgetti, MD; Alessandro Pingitore, MD, PhD; Brunella Favilli, MSc; Annette Kusch, RT; Massimo Lombardi, MD; and Paolo Marzullo, MD

Institute of Clinical Physiology, National Research Council, Pisa, Italy

The aim of this study was to compare ^{99m}Tc-tetrofosmin SPECT with contrast-enhanced MRI (ceMRI), a new direct sign of myocardial fibrosis. **Methods:** We studied 21 patients (age, 60 ± 11 y; 19 male) with previous myocardial infarction and severe left ventricular dysfunction (ceMRI EF, 29% ± 6%). All patients underwent resting and postnitrate (intravenous isosorbide dinitrate) ^{99m}Tc-tetrofosmin gated SPECT as well as ceMRI. Scintigraphic analysis was performed using quantitative perfusion SPECT (QPS), providing the percentage radiotracer uptake and defect severity in a 20-segment model. Hyperenhancement was defined by the increase of ceMRI signal intensity 20 min after intravenous injection of gadolinium–diethylenetriaminepentaacetic acid and its regional extension as the percentage of the total segment area. **Results:** In ceMRI dysfunctional segments, the correlation between the extent of hyperenhancement and both ^{99m}Tc-tetrofosmin uptake and defect severity was significantly better after nitrate administration rather than at rest ($P < 0.0001$). Using a ceMRI cutoff below 40%, 102 of 196 (52%) segments were viable, whereas 94 (48%) segments were not viable. According to receiver-operating characteristic curve analysis, diagnostic accuracies were higher for postnitrate ^{99m}Tc-tetrofosmin uptake as well as perfusion defect severity than using resting data (0.84 vs. 0.71, $P < 0.001$; 0.89 vs. 0.76, $P < 0.001$, respectively). **Conclusion:** After nitrate administration, ^{99m}Tc-tetrofosmin uptake and perfusion defect severity were closely related to ceMRI, demonstrating, in vivo, the existence of an inverse correlation between the transmural distribution of fibrosis and tracer delivery to the myocardium.

Key Words: myocardial viability; gated SPECT; contrast-enhanced MRI; nitrates

J Nucl Med 2005; 46:1285–1293

In Europe, ^{99m}Tc-labeled compounds are widely used in nuclear cardiology and their application to viability detection has progressively increased in the past several years.

Previous studies demonstrated that quantitative measures of regional tracer uptake are required to accurately predict functional recovery after revascularization (*1–3*). Alternatively, the use of nitrates before radiotracer injection seems to consistently increase regional differences in uptake, improving the nuclear cardiologists' ability to identify hibernating myocardium (*4–8*). Despite the demonstration of the clinical utility of imaging with ^{99m}Tc-labeled compounds, their extensive application when the issue is viability continues to encounter practical resistance and often other radioisotopes or scintigraphic protocols are preferred. This fact implies that we need further evidence of the power of ^{99m}Tc-labeled compounds in the assessment of myocardial viability.

MRI can identify myocardial viability with different modalities, including conventional morphologic, perfusional, and functional features (*9–12*). Moreover, experimental and clinical studies have shown that MRI can directly visualize healed myocardium with delayed-contrast imaging (contrast-enhanced MRI [ceMRI]) (*13–17*). The high spatial resolution of ceMRI and the high contrast between scar and normal tissue elicit the assessment of the transmural extent of fibrosis. Previous clinical studies have established the accuracy of ceMRI in identifying the presence, location, and transmural extent of myocardial fibrosis (*16–19*). The aim of this study was to compare ^{99m}Tc-tetrofosmin SPECT with ceMRI to provide further evidence of the clinical utility of postnitrate ^{99m}Tc-labeled compound scintigraphy in the assessment of myocardial viability in patients with severe postischemic left ventricular (LV) dysfunction.

MATERIALS AND METHODS

Patient Population

We enrolled patients with previous myocardial infarction and postischemic severe LV dysfunction. Myocardial infarction was documented with clinical history, presence of electrocardiographic Q-waves on the electrocardiogram, or typical infarctual enzymatic curve at the time of the acute event.

Patients with acute coronary artery syndrome or with LV dysfunction caused by different etiology were excluded from the study. All patients had, in random order and within 15 d: physical examination, baseline electrocardiogram and echocardiogram, ceMRI, ^{99m}Tc-tetrofosmin gated SPECT (G-SPECT) before and after nitrate administration, and coronary angiography. All patients were studied after an overnight fasting period. Nitrates were discontinued for at least 5 plasma half-lives before nitrate administration, whereas other drugs (such as angiotensin-converting enzyme inhibitors and calcium-channel blockers) were maintained.

Scintigraphic Protocol

Each patient underwent rest/postnitrate G-SPECT in a single-day protocol. Briefly, after cannulation of an antecubital vein, ^{99m}Tc-tetrofosmin (296–370 MBq) was administered intravenously in the resting condition. Fifteen minutes later, patients ate a fatty meal to accelerate tracer hepatopathobiliary clearance. About 45 min after radiotracer injection, a resting G-SPECT study was performed using a double-head γ-camera (ECam; Siemens) equipped with high-resolution collimators. A 64 × 64 matrix, 32 projections, 40-s projections, 8 frames/cycle protocol was used in association with a 15% window centered on the 140-keV photopeak of ^{99m}Tc. The study was reconstructed using filtered backprojection without attenuation or scatter correction. Immediately after completion of the baseline study, nitrate infusion began (isosorbide dinitrate [ISDN], 0.2 mg/mL, 10 mL/h). Criteria for radiotracer injection were a drop in systolic blood pressure (≥20 mm Hg vs. rest systolic blood pressure) or an increase in heart rate (>20 bpm vs. rest heart rate). In the absence of evidence of a hemodynamic effect, nitrate infusion was maintained for at least 20 min. ^{99m}Tc-Tetrofosmin (740–888 MBq) was administered thereafter, continuing the nitrate infusion for at least 2 min. Afterward, the acquisition protocol described for baseline G-SPECT was repeated. A 12-lead electrocardiogram and blood pressure were monitored throughout the entire duration of the study.

An operator-independent analysis of scintigraphic data (regional wall motion [WM] and wall thickening) was performed using previously validated software for quantitative perfusion SPECT analysis (QGS; E.Soft) (20). Briefly, this is an automatic quantitative algorithm for the measurement of regional myocardial WM and wall thickening from 3-dimensional gated myocardial perfusion SPECT images. The algorithm measures the motion of the 3-dimensional endocardial surface using a modification of the centerline method as well as wall thickening using both geometry (gaussian fit) and partial volume (counts) and providing scores of regional WM (from 0 = normal to 5 = dyskinesis) and wall thickening (from 0 = normal to 3 = absent thickening) in a 20-segment polar map. Regional myocardial dysfunction was automatically identified by considering a WM QGS score of >2 or a wall thickening QGS score of >2. Regional perfusion was assessed by means of quantitative perfusion SPECT (QPS) providing, automatically, the percentage of regional uptake of ^{99m}Tc-tetrofosmin and defect severity (0–10 SDs below the healthy patients' database) in the same 20-segment polar map.

MRI

MRI was performed using a 1.5-T whole-body MR scanner (CVi; GE Healthcare) equipped with a high-performance gradient (40-mT/m amplitude, 150-mT ms^{-1} slew rate) and a multichannel receiver with a maximal bandwidth of 250 kHz. A 4-element (2 anterior and 2 posterior) cardiac phased-array receiver surface coil was used for signal reception. Patients were placed on the imaging table, feet first in supine position with cushions under the knees and feet. A breath-hold segmented gradient-echo fast imaging, using steady-state acquisition, electrocardiographically triggered sequence was used for the evaluation of regional and contractile function. The following parameters were used: echo time (TE), 1.7 ms; repetition time, 4.0 ms; slice thickness, 8 mm with no inter-slice gap; field of view (FOV), 320 mm; data matrix size, 256 × 224 mm; phase of field, 0.75; trigger delay, the minimum; views per segment, 8–14 according to the heart rate; flip angle, 45°. A minimum of 40 cine frames was obtained for each slice. Postcontrast delayed images were acquired in the short axis of the LV 20 min after bolus injection of 0.2 mmol/kg of gadolinium–diethylenetriaminepentaacetic acid (Gd-DTPA) in end-diastole for the evaluation of myocardial distribution of hyperenhancement (HE). A gradient-echo inversion recovery sequence was used with the following parameters: TE, 4.2 ms; flip angle, 20°; matrix, 256 × 160; number of excitations, 2.00; FOV, 36 mm; slice thickness, 10 mm. The inversion time ranged from 220 to 300 ms. A real-time option, which allowed the interactive change of inversion time, was used to optimize this parameter until nulling of the myocardium was obtained. A variable number of short-axis slices (10 ± 1.8; maximum, 11; minimum, 8) have been traced from the base to the apex to cover the entire LV. To assess the apex, vertical and horizontal long-axis views (one of each) were also acquired.

MRI LV Function Assessment. LV function was evaluated by consecutive cine short-axis views from the mitral valve plane to the apex. Four- and 2-chamber views were acquired for evaluation of the apex. LV manual drawing of the endocardial contour in end-systolic and end-diastolic short-axis frames was obtained using a commercial postprocessing program (Massanalysis) on an independent Sun Sparc Station (Sun Microsystems) to calculate LV volumes and ejection fraction (EF). WM was qualitatively evaluated by dividing the LV according to the same 20-segment model as that used for SPECT, including 6 basal, middle, and distal wall segments and the anterior and inferior apex. The semiautomatic segmentation started from the right ventricle interception that was used as an anatomic marker to provide the best correspondence of myocardial regions. WM was graded as follows: 1 = normal, 2 = hypokinetic, 3 = akinetic, 4 = dyskinetic. A WM score index was derived by dividing the sum of individual segment scores by the number of segments. The analysis was done by 2 expert cardiologists who were unaware of each other's findings.

Delayed-Contrast Enhancement for Myocardial Necrosis Assessment. Nonviable tissue was identified on the 20-min image after administration of Gd-DTPA. In each of the 20 segments, the total and the hyperenhanced areas were identified automatically by a specific software and were manually corrected if needed by 2 operators who were unaware of each other's findings. The segmental extent of HE within each segment was calculated as the percentage of the total segment area, according to the following formula: HEA (%) = (HEA × 100)/(HEA + NEA), where HEA is the hyperenhanced area and NEA in the nonhyperenhanced area (15). Intra- and interobserver variabilities were 0.94 and 0.97, respectively ($P < 0.0001$).

Coronary Angiography and Left Ventriculography

Standard coronary angiography and single-plane contrast ventriculography were performed in multiple views within 2 wk of the scintigraphic study. All angiograms were qualitatively and quantitatively (GE Healthcare software) evaluated by 2 physicians who

were unaware of the protocol study. Stenoses of >50% were considered significant. All patients had a dominant right coronary artery.

Statistical Analysis

Continuous variables are presented as mean ± SD. Where indicated, differences were assessed by the Student t test for paired or unpaired data. The significance of the relationship between both regional myocardial percentage uptake of ^{99m}Tc-tetrofosmin and defect severity, at rest and after nitrates, and regional HE was assessed by linear regression analysis. Analysis of agreement was also performed using the Bland–Altman method (21). Accuracy in myocardial viability detection for both resting and postnitrate ^{99m}Tc-tetrofosmin was estimated by receiver-operating-characteristic (ROC) curve analysis, using MedCalc Software. κ-statistics and its SE were calculated to assess the agreement between ^{99m}Tc-tetrofosmin scans and ceMRI scans in the identification of myocardial viability. κ-values < 0.4, between 0.4 and 0.75, and >0.75 were taken to represent poor, fair-to-good, and excellent agreement, respectively (22). Statistical significance for all analyses was assessed at $P < 0.05$.

RESULTS

Clinical Results

The study included 21 patients (mean age, 60 ± 11 y; 19 male, 2 female) with previous Q-wave myocardial infarction (8 anterior, 10 inferior, 3 anterior and inferior) and postischemic severe LV dysfunction (ceMRI EF = 29% ±

6%). The mean time interval between myocardial infarction and SPECT was 41 ± 70 mo (range, 4–240 mo). Eleven patients had mild and 7 had moderate mitral insufficiency.

At rest, the mean rate·pressure product was 9,125 ± 1,729 mm Hg·bpm and did not change significantly after nitrates (9,624 ± 1,923 mm Hg·bpm; P = not significant [NS]). Resting G-SPECT EF (32% ± 5%) correlated with ceMRI (29% ± 6%; $r = 0.47$, $P < 0.03$), whereas it did not correlate with contrast ventriculography (32% ± 6%; $r = 0.05$, P = NS). Similarly, resting G-SPECT end-diastolic LV volumes (197 ± 62 mL) correlated well with ceMRI (215 ± 78 mL; $r = 0.64$, $P < 0.002$), whereas they did not correlate well with angiographic results (272 ± 66 mL; $r = 0.08$, P = NS). Three patients had single-vessel, 7 patients had double-vessel, and 11 patients had triple-vessel coronary disease. Three patients received thrombolytic therapy at the time of myocardial infarction, 3 patients submitted to percutaneous transluminal coronary angioplasty (PTCA), and 3 submitted to coronary artery bypass graft (CABG). Clinical data are summarized in Table 1.

Scintigraphic Results

In analysis of SPECT perfusion at rest and after nitrate administration, 420 segments were analyzed; 196 (46%) were dysfunctional on ceMRI WM analysis, whereas the remaining 224 showed normal regional function. In these

TABLE 1
Clinical, Angiographic, Scintigraphic, and MRI Data

Patient no.	Sex	Age (y)	MRI EF	MRI edv	CV EF	CV edv	G-SPECT EF	G-SPECT edv	Coronary angiography DA	CX	RC	PMI	Thrombo	PTCA	CABG
1	M	57	31	200	41	399	31	198	100	0	100	ANT	No	Yes	No
2	M	81	33	137	35	256	31	200	75	75	0	ANT + INF	No	No	No
3	M	76	20	300	33	198	33	157	75	90	100	INF	No	No	No
4	M	47	35	112	32	140	36	112	99	0	50	ANT	Yes	No	No
5	M	61	32	196	38	399	32	196	100	75	100	ANT	No	No	No
6	M	76	34	171	—	—	37	171	0	0	90	INF	No	No	No
7	M	38	35	112	38	175	38	181	60	75	100	INF	No	No	No
8	M	54	23	383	29	397	23	383	90	75	90	ANT	No	Yes	No
9	F	58	35	280	35	280	37	180	75	0	75	ANT	No	No	No
10	M	49	31	168	—	—	31	168	90	0	0	ANT	No	Yes	No
11	M	51	16	299	23	241	21	310	90	90	90	ANT + INF	No	No	No
12	M	53	25	225	25	268	25	225	75	75	100	INF	No	No	No
13	M	52	18	324	18	398	20	185	75	0	100	ANT	Yes	No	No
14	M	59	21	142	39	286	31	142	100	75	75	INF	No	No	No
15	M	60	30	175	30	200	35	175	50	0	90	INF	Yes	No	No
16	M	78	30	160	35	249	34	160	90	90	75	INF	No	No	No
17	M	75	36	254	28	260	36	254	90	75	90	INF	No	No	Yes
18	F	57	38	160	35	194	35	180	99	0	0	ANT	No	No	No
19	M	66	34	278	22	402	38	145	50	50	100	INF	No	No	No
20	M	54	27	262	28	232	31	262	100	0	100	ANT + INF	No	No	Yes
21	M	62	32	155	35	195	34	155	90	100	100	INF	No	No	Yes

CV = contrast ventriculography; EF = ejection fraction; edv = end-diastolic volume; DA = descending anterior coronary artery; CX = circumflex coronary artery; RC = right coronary artery; PMI = previous myocardial infarction; Thrombo = thrombolysis; ANT = anterior; INF = inferior.

latter segments, the mean regional percentage ^{99m}Tc-tetrofosmin uptake at rest was 67.4% ± 15% and increased significantly after nitrate administration (78.4% ± 15%; $P < 0.001$). Similarly, the mean perfusion defect severity at rest was 2.85 ± 1.5 SD and decreased significantly after nitrate infusion (0.69 ± 1.02 SD; $P < 0.001$).

In regions with resting impaired ventricular function, linear regression analysis showed a good correlation between the resting and postnitrate percentage uptake of ^{99m}Tc-tetrofosmin ($y = 1.073x + 5.13$; $r = 0.84$; SEE = 11.5; $P < 0.0001$) as well as a good inverse relation between the resting and postnitrate defect severity ($y = 1.092x − 1.69$; $r = 0.83$; SEE = 1.82; $P < 0.0001$; Fig. 1). The quantitative agreement between the flow data in the 2 conditions was also analyzed by means of the Bland–Altman method, which resulted in a mean increase in the percentage postnitrate ^{99m}Tc-tetrofosmin uptake of 8.49% ± 11.6%, with a 95% confidence interval (CI) of −14.56% to 31.52% (Fig. 1). In terms of the perfusion defect severity,

the Bland–Altman method showed a mean decrease in postnitrate ^{99m}Tc-tetrofosmin SDs below normal values of −1.250 ± 1.83 SD, resulting in a 95% CI of −4.91 SD to 2.41 SD (Fig. 1).

SPECT Versus ceMRI Data

Regional ^{99m}Tc-Tetrofosmin Uptake. In regions with preserved function at rest, the segmental extent of HE averaged 3.0% ± 10%. In regions with resting dysfunction, the correlation between the segmental extent of HE and the regional percentage of ^{99m}Tc-tetrofosmin uptake was closer to postnitrate than to resting perfusion data ($r = 0.82$ [SEE = 11.97] vs. 0.66 [SEE = 12.34]; $P < 0.0001$) (Fig. 2). Using a ceMRI cutoff below 40%, derived from previously published data (*23*), as the one providing the highest diagnostic accuracy for the detection of myocardial viability, 102 (52%) segments were viable, whereas 94 (48%) were nonviable. The regional ^{99m}Tc-tetrofosmin percentage uptake was higher in ceMRI viable segments than in nonviable
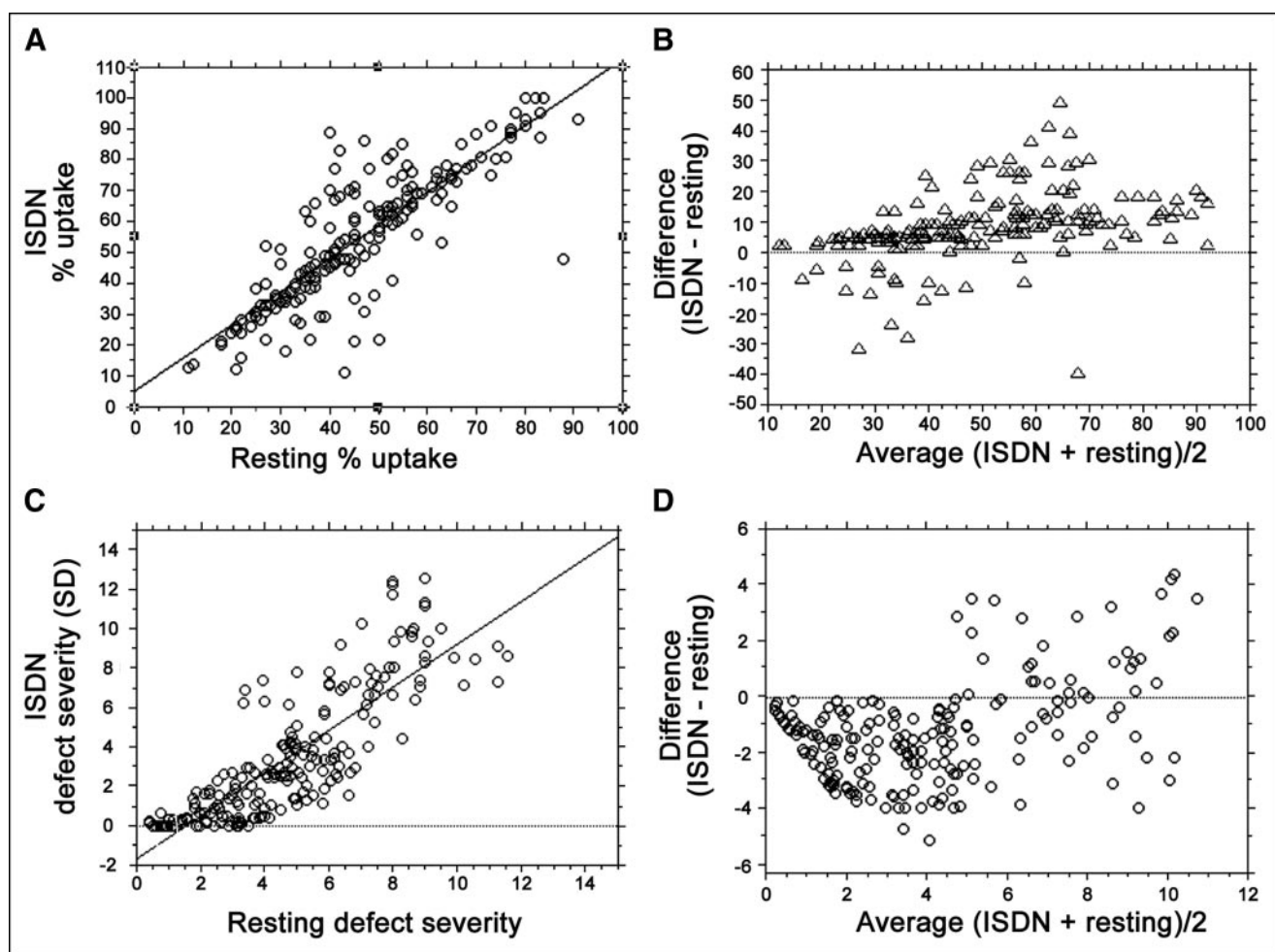

FIGURE 1. In segments with baseline impaired LV function, linear regression analysis resulted in good correlation between resting and postnitrate ^{99m}Tc-tetrofosmin uptake (A) ($y = 1.073x + 5.13$; $r = 0.84$; $P < 0.0001$) as well as perfusion defect severity (C) ($y = 1.092x − 1.69$; $r = 0.83$; $P < 0.0001$). The Bland–Altman method, which plots the difference vs. the average of the measures, demonstrated a mild shift toward positive percentage uptake values (B) and a mild decrease in perfusion defect severity (D), suggesting an amelioration of regional perfusion after nitrate administration.
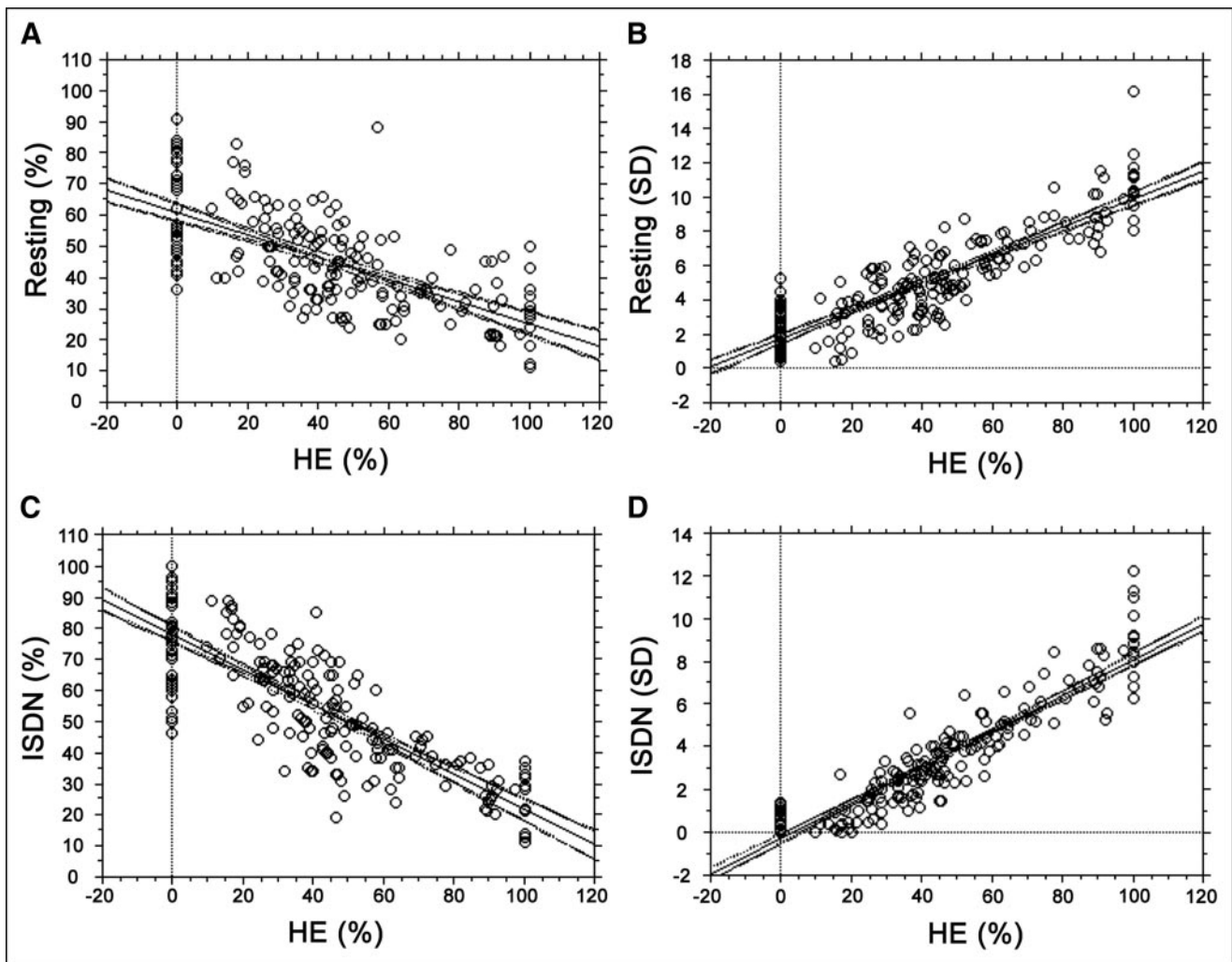
FIGURE 2. Regression plots with 95% confidence bands. In regions with resting dysfunction, correlation between the segmental extent of HE and regional percentage ^{99m}Tc-tetrofosmin uptake was closer to postnitrate data (C) than to resting perfusion data (A) ($r = 0.82$ vs. 0.66; $P < 0.0001$). Similarly, linear regression analysis revealed a better relationship between regional HE and postnitrate (D) than perfusion defect severity at rest (B) ($r = 0.93$ vs. 0.86; $P < 0.0001$).

segments at rest (55% ± 15% vs. 38% ± 12%; $P < 0.001$) and increased significantly after nitrates in ceMRI viable areas (69% ± 15%; $P < 0.001$), whereas it did not in ceMRI nonviable areas ($P = $ NS; Fig. 3). ROC curve analysis identified cutoffs of 40% for resting ^{99m}Tc-tetrofosmin uptake and 51% for postnitrate imaging as the best cutoffs separating viable from nonviable tissue (Fig. 3). Using these thresholds, resting ^{99m}Tc-tetrofosmin percentage uptake predicted myocardial viability in 88 of 102 segments (0.86, sensitivity) and scarring in 53 of 94 segments (0.56, specificity) with 0.71 global accuracy (Fig. 4). In postnitrate ^{99m}Tc-tetrofosmin scans, sensitivity, specificity, and global accuracy were 0.89, 0.78, and 0.84, respectively. The area under the ROC curve was significantly greater for postnitrate data compared with resting SPECT data: 0.90 (95% CI, 0.85–0.94) versus 0.80 (95% CI, 0.74–0.86) ($P < 0.001$). Moreover, κ-statistics showed that the agreement with ceMRI was significantly higher using post-

nitrate data than the baseline cutoff (κ = 0.67, SE = 0.05 vs. κ = 0.41, SE = 0.06; $P < 0.01$).

Regional ^{99m}Tc-Tetrofosmin Perfusion Defect Severity. In terms of perfusion defect severity, the regional extent of HE correlated more with postnitrate than with resting data ($r = 0.93$ [SEE = 0.99] vs. 0.86 [SEE = 1.41]; $P < 0.0001$) (Fig. 2). The perfusion defect severity at rest was lower in ceMRI viable segments than in nonviable segments (3.2 ± 1.6 SD vs. 6.7 ± 2.3 SD; $P < 0.001$) and decreased significantly after nitrates in ceMRI viable areas (1.16 ± 1.2 SD; $P < 0.001$), whereas it did not change in ceMRI nonviable areas ($P = $ NS) (Fig. 3). ROC curve analysis identified cutoffs of 3.18 SD and 2.5 SD for resting and postnitrate perfusion defect severity, respectively, as the best cutoffs separating viable from nonviable tissue (Fig. 3). Using these thresholds, resting perfusion defect severity predicted myocardial viability in 94 of 102 segments (0.92, sensitivity) and scarring in 56 of 94 segments (0.60, spec-
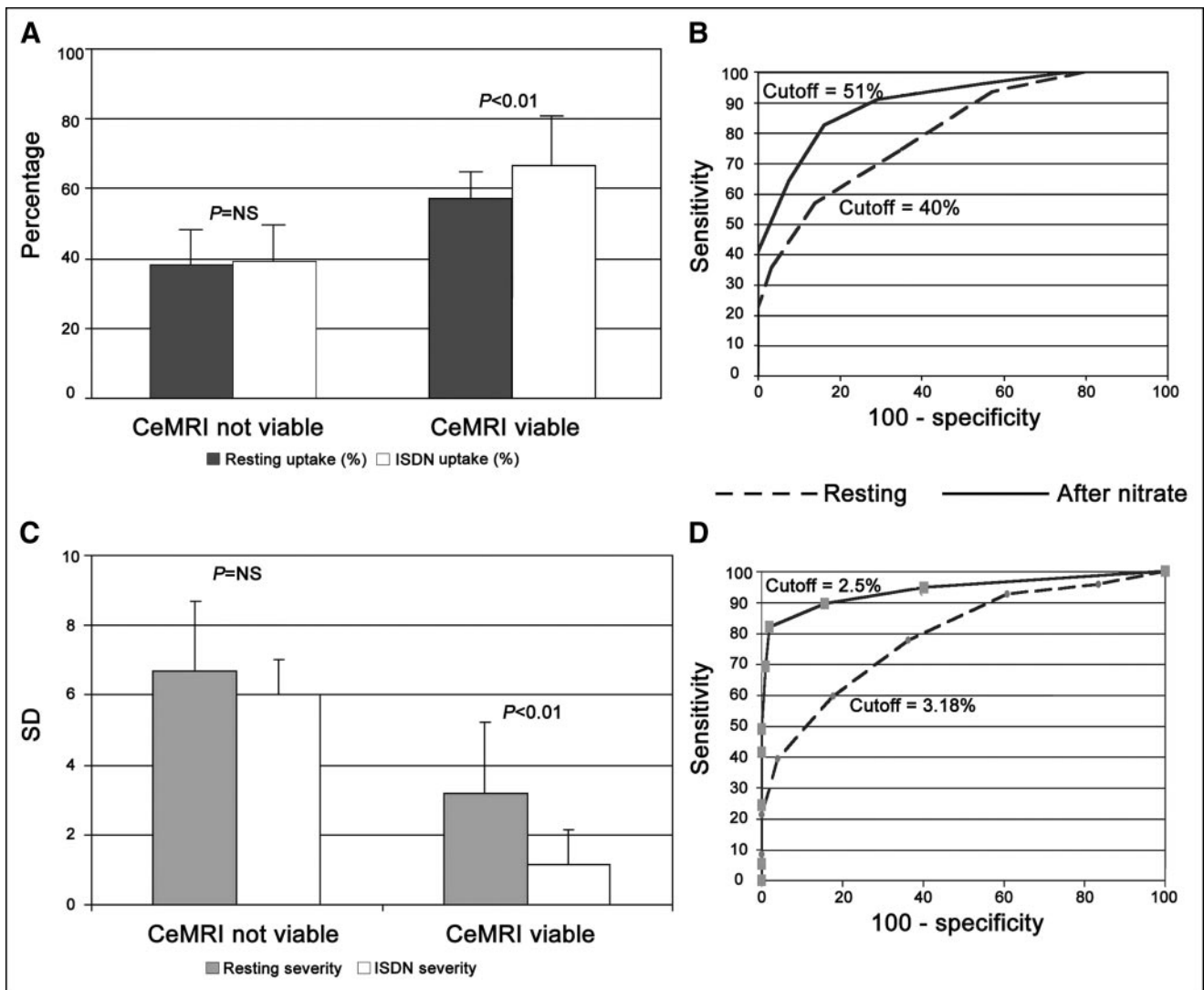
FIGURE 3. Mean regional ^{99m}Tc-tetrofosmin percentage uptake was higher in ceMRI viable segments than in nonviable segments at rest and increased significantly after nitrates in ceMRI viable areas, whereas it did not in ceMRI nonviable areas (A). ROC curve analysis showed that the area under the ROC curve was significantly greater for postnitrate data compared with resting SPECT data (B). Similar results were obtained in terms of perfusion defect severity (C and D).

ificity) with a global accuracy of 0.76 (Fig. 4). In postnitrate imaging, sensitivity, specificity, and global accuracy were 0.94, 0.86, and 0.89, respectively (Fig. 4). The area under the ROC curve was significantly greater in postnitrate data compared with resting SPECT data: 0.96 (95% CI, 0.93–0.99) versus 0.89 (95% CI, 0.84–0.95) ($P < 0.001$) (Fig. 4). Furthermore, the κ-statistic showed that the agreement with ceMRI was significantly higher using the postnitrate cutoff than the baseline cutoff (κ = 0.78 [SE = 0.03] vs. κ = 0.44 [SE = 0.03]; $P < 0.01$).

DISCUSSION

To our knowledge, this is the first study exploring the ability of semiquantitative rest/postnitrate ^{99m}Tc-tetrofosmin SPECT compared with ceMRI in the detection of myocardial viability. Our results confirm and expand previous

observations demonstrating that postnitrate ^{99m}Tc-tetrofosmin imaging accurately depicts myocardial viability when it is also investigated using an independent marker of myocardial fibrosis with high spatial resolution, such as ceMRI.

ceMRI for Myocardial Viability Assessment

ceMRI has recently been proposed as an alternative modality for the assessment of myocardial viability, further providing direct visualization of the transmural extent of viable and nonviable tissue. Previous experimental studies showed that ceMRI depicts directly and specifically healed myocardium and that the extent of HE matches closely the extent of necrosis that is documented histologically (13,14). Using the high spatial resolution of MRI, Fieno et al. demonstrated in animal studies that the size and the shape of hyperenhanced regions reproduced the areas of irreversible
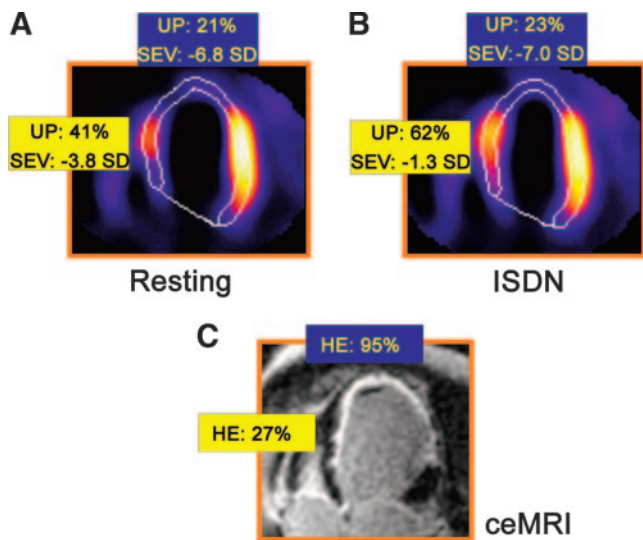
FIGURE 4. Scintigraphic images (A and B) and ceMRI transverse images (C) of patient 18 with previous myocardial infarction of anterior wall involving interventricular septum. After nitrate administration, regional perfusion increased in interventricular septum (as demonstrated by increase in radiotracer uptake and decrease in perfusion defect severity), whereas it did not change in anterior wall. ceMRI showed inverse and congruent results demonstrating extensive fibrosis of anterior wall and persistence of myocardial viability in interventricular septum. UP = percentage of ^{99m}Tc-tetrofsmin uptake; SEV = perfusion defect severity.

injury defined by tetrazolium staining (*14*). The transmural extent of delayed enhancement has been shown to be predictive of regional recovery of function after revascularization procedures in experimental studies (*15*) and in patients with acute myocardial infarction as well as in those with chronic ischemic heart disease (*17,24*). Recently, Kuhl et al. demonstrated that segmental glucose uptake by PET was inversely correlated with the extent of HE (*23*). By ROC curve analysis, a cutoff value of 37% for segmental extent of enhancement optimally differentiated viable from nonviable segment. Using this threshold, the sensitivity and specificity of ceMRI to detect myocardial viability as defined by PET were 0.96 and 0.84, respectively (*24*). Therefore, ceMRI allows detection of viable myocardium with a high accuracy as compared with morphologic, functional, and metabolic indices of myocardial viability.

Postnitrate ^{99m}Tc-Labeled Compounds for Myocardial Viability Identification

In past years, the role of ^{99m}Tc tracers in myocardial viability assessment has been widely debated and several studies reported the possibility of the underestimation of viability in resting conditions unless a quantitative analysis of regional radiotracer uptake is undertaken (*1–3*). To overcome the limited diagnostic power of ^{99m}Tc-labeled compounds in distinguishing hypoperfused but still viable myocardium from scarring, a modified protocol using nitrate administration has been proposed (*4–8*). Nitrate SPECT has

been shown to predict postrevascularization recovery of LV function better than rest studies (*4–7*) and to provide important prognostic information (*25*). More recently, we demonstrated that resting and postnitrate scintigraphic data could be arranged in a kind of perfusional mismatch similar to a PET flow/metabolic mismatch (*8*). These studies showed a wide variability in the modality of nitrate administration (sublingual or intravenous infusion) and in the classification of the relative perfusion changes. However, no matter which algorithm is used, nitrates ameliorated diagnostic accuracy in the detection of myocardial viability, providing clinical information similar to that of other radioisotopic approaches or other techniques. Despite demonstration of the clinical utility of imaging with postnitrate ^{99m}Tc-labeled compounds, when the issue is viability, their extensive application continues to have a limited clinical application and dual isotopes ^{201}Tl/^{99m}Tc-labeled compounds imaging is usually used. This fact implies that further evidence of the power of ^{99m}Tc-labeled compounds in the assessment of myocardial viability is needed.

Postnitrate ^{99m}Tc-Tetrofosmin Scintigraphy Versus ceMRI

The results of this study compare favorably with previous reports demonstrating that, when using an independent marker of fibrosis such as ceMRI, postnitrate scintigraphic imaging better depicts the presence and the transmural extent of myocardial viability than the resting scan. Indeed, our resting data, either as regional percentage ^{99m}Tc-tetrofosmin uptake or perfusion defect severity, underestimated myocardial viability when compared with postnitrate results. These latter data showed a significantly better correlation with regional distribution of HE, resulting in a higher diagnostic accuracy by ROC curve analysis, whereas the κ-statistic demonstrated a good agreement with the ceMRI definition of myocardial viability. For both percentage tracer uptake and perfusion defect severity, the increase in diagnostic accuracy after nitrate administration resulted from an improvement in specificity and, therefore, from the reduction of the number of "false necrotic" segments. This phenomenon reflects the effect of nitrates that, through local and systemic mechanisms (*26–28*), increases regional blood flow and, thus, the amount of tracer delivered to the asynergic areas and taken up by viable myocytes. Alternatively, the reduced workload in control, reference regions might have smoothed perfusion differences among different ventricular segments (*29*). On the other hand, about 22% of ceMRI nonviable segments showed a postnitrate percentage uptake of >51% and, in this case, relative segmental counts on the SPECT images might provide a better estimate of the true volume of viable tissue in that myocardial segment.

These false viable areas could account for the limited sensitivity of myocardial scintigraphy in studies in which the gold standard is postrevascularization recovery of function. Indeed, the extent or the localization of fibrosis in the myocardial wall (i.e., patchy or in the subendocardial lay-

ers), as documented by ceMRI, might prevent the recovery of function after revascularization, despite the persistence of tracer uptake. Therefore, it is possible to represent myocardial viability according to different spatial coordinates: circumferentially, that is the number of necrotic segments, and, transmurally, the extent of necrosis from the subendocardium to subepicardium. The transmural stratification of viability introduces the hypothesis that viability may be considered as not a dichotomous variable, which is present or absent according to the actual perfusional and functional criteria. Rather, viability could be a continuous variable in which extremes are represented by full transmural viability without any scar and full necrosis without viability. The correlated scenarios are the spontaneous or postrevascularization recovery of contractile function or the absence of it. In the middle, at a different degree of mixture, the coexistence of viable and scar tissue could influence the ability of our techniques to correctly categorize myocardial viability and, thus, our capability to perform adequate therapeutic strategies for improving patients' outcome.

Limitations

This study had several limitations. The lack of follow-up prevented us from investigating the correlation between myocardial viability assessed by ^{99m}Tc-tetrofosmin and functional recovery after revascularization. On these bases, ceMRI cannot be considered as an absolute standard. Nevertheless, the purpose of this study was to compare, in vivo, rest and postnitrate scintigraphic imaging with an independent marker of myocardial fibrosis. In our study, the postnitrate results appeared to be closely correlated with ceMRI data and likely with ceMRI diagnostic previously published implications.

Anatomic misalignment can account for discrepancies between SPECT and ceMRI.

Technical factors, as inversion delay time (from the contrast injection to the image acquisition) and the acquisition time (from the contrast injection to the image acquisition), can influence the presence and extent of HE (*30*). We adopted a standardized protocol in all patients in relation to the contrast dose and the acquisition time. Moreover, we performed 3–5 proofs to optimize inversion delay time before starting the acquisition.

In determining diagnostic accuracy using ^{99m}Tc-tetrofosmin perfusion alone, rigid cutoff values were applied, without any normalization for the site of perfusion defect and the degree of regional dysfunction. However, despite the poor diagnostic accuracy obtained, our data were very similar to those by other authors using different cutoff values and regional normalization.

Our study protocol used intravenous nitrate administration, which could appear almost complex for the logistic of a nuclear cardiology laboratory. Nevertheless, this protocol is not very different from a stress–rest study.

Finally, although each subject was completely characterized by clinical, angiographic, echocardiographic, and ra-

dioisotopic techniques, the study group was limited to 21 patients.

CONCLUSION

After nitrate administration, the percentage ^{99m}Tc-tetrofosmin uptake and scintigraphic perfusion defect severity were closely related to the transmural distribution of HE, demonstrating, in vivo, the existence of an inverse correlation between the distribution of fibrosis and tracer delivery to the myocardium. Our data confirm and expand previous observations showing that, in patients with postischemic severe LV dyfunction, postnitrate imaging is a useful and accurate tool to assess myocardial viability.

REFERENCES

1. Maes AF, Borgers M, Flameng W, et al. Assessment of myocardial viability in chronic coronary artery disease using technetium-99m sestamibi SPECT: correlation with histologic and positron emission tomographic studies and functional follow-up. *J Am Coll Cardiol.* 1997;29:62–68.

2. Udelson JE, Coleman PS, Metherall J, et al. Predicting recovery of severe regional ventricular dysfunction: comparison of resting scintigraphy with ^{201}Tl and ^{99m}Tc-sestamibi. *Circulation.* 1994;89:2552–2561.

3. Dakik HA, Howell JF, Lawrie GM, et al. Assessment of myocardial viability with ^{99m}Tc-sestamibi tomography before coronary artery by-pass graft surgery: correlation with histopathologic and postoperative improvement in cardiac function. *Circulation.* 1997;96:2982–2988.

4. Galli M, Marcassa C, Imparato A, Campini R, Orrego PS, Giannuzzi P. Effect of nitroglycerin by technetium-99m sestamibi tomoscintigraphy on resting regional myocardial hypoperfusion in stable patients with healed myocardial infarction. *Am J Cardiol.* 1994;74:843–848.

5. Bisi G, Sciagra R, Santoro GM, Fazzini PF. Rest technetium-99m sestamibi tomography in combination with short-term administration of nitrates: feasibility and reliability for prediction of postrevascularization outcome of asynergic territories. *J Am Coll Cardiol.* 1994;24:1282–1289.

6. Li ST, Liu XJ, Lu ZL, et al. Quantitative analysis of technetium 99m-methoxyisobutyl isonitrile single-photon emission computer tomography and isosorbide dinitrate infusion in assessment of myocardial viability before and after revascularization. *J Nucl Cardiol.* 1996;3:457–463.

7. Flotats A, Carrio I, Estorch M, et al. Nitrate administration to enhance the detection of myocardial viability by technetium-99m tetrofosmin single photon emission tomography. *Eur J Nucl Med.* 1997;24:767–773.

8. Giorgetti A, Marzullo P, Sambuceti G, et al. Baseline/post-nitrate ^{99m}Tc-tetrofosmin mismatch for the assessment of myocardial viability in patients with severe left ventricular dysfunction: comparison with baseline ^{99m}Tc-tetrofosmin scintigraphy/^{18}FDG-positron emission tomography imaging. *J Nucl Cardiol.* 2004;11:142–151.

9. Baer FM, Voth E, Schneider CA, Theissen P, Schicha H, Sechtem U. Comparison of low dose dobutamine gradient echo magnetic resonance imaging and positron emission tomography with ^{18}F fluorodeoxyglucose in patients with chronic coronary artery disease: a functional and morphological approach to the detection of residual myocardial viability. *Circulation.* 1995;91:1006–1015.

10. van Rugge FP, van der Wall EE, van Dijkman PR, Louwerenburg HW, de Roos A, Bruschke AV. Usefulness of ultrafast magnetic resonance imaging in healed myocardial infarction. *Am J Cardiol.* 1992;70:1233–1237.

11. Geskin G, Kramer CM, Rogers WJ, et al. Quantitative assessment of myocardial viability after infarction by dobutamine magnetic resonance tagging. *Circulation.* 1998;98:217–223.

12. Gunning MA, Anagnostopoulos C, Knight CJ, et al. Comparison of ^{201}Tl, ^{99m}Tc-tetrofosmin, and dobutamine magnetic resonance imaging for identifying hibernating myocardium. *Circulation.* 1998;98:1869–1874.

13. Kim RJ, Fieno DS, Parrish TB, et al. Relationship of MRI delayed contrast enhancement to irreversible injury, infarct age, and contractile function. *Circulation.* 1999;100:1992–2002.

14. Fieno DS, Kim RJ, Chen EL, Lomasney JW, Klocke FJ, Judd RM. Contrast enhanced magnetic resonance imaging of myocardium at risk: distinction between reversible and irreversible injury throughout infarct healing. *J Am Coll Cardiol.* 2000;36:1985–1991.

15. Hillenbrand HB, Kim RJ, Parker MA, Fieno DS, Judd RM. Early assessment of myocardial salvage by contrast-enhanced magnetic resonance imaging. *Circulation.* 2000;102:1678–1683.

16. Klein C, Nekolla SG, Bengel FM, et al. Assessment of myocardial viability with contrast enhanced magnetic resonance imaging: comparison with positron emission tomography. *Circulation.* 2002;105:162–167.

17. Kim RJ, Wu E, Rafael A, et al. The use of contrast enhanced magnetic resonance imaging to identify reversible myocardial dysfunction. *N Engl J Med.* 2000;343:1445–1453.

18. Wu E, Judd RM, Vargas JD, Klocke FJ, Bonow RO, Kim RJ. Visualization of presence, location, and transmural extent of healed Q-wave and non-Q-wave myocardial infarction. *Lancet.* 2001;357:21–28.

19. Ramani K, Judd RM, Holly TA, et al. Contrast magnetic resonance imaging in the assessment of myocardial viability in patients with stable coronary artery disease and left ventricular dysfunction. *Circulation.* 1998;98:2687–2694.

20. Germano G, Erel J, Lewin H, et al. Automatic quantitation of regional myocardial wall motion and thickening from gated technetium-99m sestamibi myocardial perfusion single-photon emission computed tomography. *J Am Coll Cardiol.* 1997;30:1360–1367.

21. Bland JM, Altman DG. Statistical methods for assessing agreement between two methods of clinical assessment. *Lancet.* 1986;1:307–310.

22. Fleiss J. *Statistical Methods for Rates and Proportions.* 2nd ed. New York, NY: Wiley & Sons; 1981.

23. Kuhl HP, Beek AM, van der Weedt AP, et al. Myocardial viability in chronic ischemic heart disease: comparison of contrast-enhanced magnetic resonance imaging with ^{18}F-fluorodeoxyglucose positron emission tomography. *J Am Coll Cardiol.* 2003;41:1341–1348.

24. Choi KM, Kim RJ, Gubernikoff G, et al. Transmural extent of acute myocardial infarction predicts long-term improvement in contractile function. *Circulation.* 2001;104:1101–1107.

25. Sciagrà R, Pellegri M, Pupi A, et al. Prognostic implications of Tc-99m sestamibi viability imaging and subsequent therapeutic strategy in patients with chronic coronary artery disease and left ventricular dysfunction. *J Am Coll Cardiol.* 2000;36:739–745.

26. Winbury MM. Redistribution of left ventricular blood flow produced by nitroglycerin: an example of integration of the macro- and microcirculation. *Circ Res.* 1971;28(suppl I):140–147.

27. Fujita M, Yamanishi K, Hirai T, et al. Significance of collateral circulation in reversible left ventricular asynergy by nitroglycerin in patients with relatively recent myocardial infarction. *Am Heart J.* 1990;120:521–528.

28. Abrams J. Mechanisms of action of the organic nitrates in the treatment of myocardial ischemia. *Am J Cardiol.* 1992;70:30B–42B.

29. Tadamura E, Mamede M, Kubo S, et al. The effect of nitroglycerin on myocardial blood flow in various segments characterized by rest-redistribution thallium SPECT. *J Nucl Med.* 2003;44:745–751.

30. Oshinski JN, Yang Z, Jones JR, Mata JF, French BA. Imaging time after Gd-DTPA injection is critical in using delayed enhancement to determine infarct size accurately with magnetic resonance imaging. *Circulation.* 2001;104:2838–2842.